Slow sound based delay-line acoustic metamaterial

M. Malléjac, P. Sheng, V. Tournat, V. Romero-García, J.-P. Groby

Slow sound based delay-line acoustic metamaterial

M. Malléjac,[1,*] P. Sheng,[2] V. Tournat,[1] V. Romero-García,[1] and J.-P. Groby[1]

[1]*Laboratoire d'Acoustique de l'Université du Mans (LAUM), UMR 6613, Institut d'Acoustique - Graduate School (IA-GS), CNRS, Le Mans Université, France*

[2]*Department of Physics, HKUST, Clear Water Bay, Kowloon, Hong Kong, China*

(Dated: February 9, 2022)

Abstract

Periodic structures composed of quarter-wavelength or Helmholtz resonators have been widely used in the design of acoustic metamaterials. An interesting phenomenon achievable through hybridization in such structures is the slow sound, which results from the strong dispersion produced by the local resonances. It gives rise to many applications such as deep sub-wavelength sound absorbers or metadiffusers. All the applications proposed so far have been analyzed only in the frequency domain (steady state). In this work, we propose a passive treatment that can be used in room acoustics, which requires considering the time domain and all multiple reflections. We analytically design a delay line from a metasurface made of Helmholtz resonators, using slow sound propagation. We prove numerically and experimentally that such structures can delay a pulse and thus reproduce the sound perception of a propagation over a given distance, larger than the actual size of the treatment. The limitations of real-time pulse propagation, dispersion, and losses on audio fidelity are discussed.

The control of acoustic waves for room acoustics applications has been of constant interest for centuries, for two main purposes: to control diffusion and to enhance absorption. From the first Helmholtz resonators used in antique amphitheaters and the Shroeder's diffusers principle [1], a long road has been traveled to more sophisticated systems such as active electroacoustic devices [2, 3], virtual sources and immersive boundaries [4–7], optimized graded porous materials [8], or acoustic metasurfaces and metamaterials [9–14]. The great advantage of the latter is that they offer the possibility of tackling the device thickness/frequency paradigm. A thickness greater than the quarter of the acoustic wavelength is usually required to attain a good efficiency for both phenomena, absorption or diffusion. In particular, Yang *et al.* defined a causality-dictated inequality stating the optimal absorption spectrum as a function of sample thickness [15], which inevitably leads to a compromise between working frequency bandwidth and thickness. It is worth noting here, that recently, Mak *et al.* proposed a new design based on soft boundaries to go beyond this causal limit [16].

The search for deep sub-wavelength sound absorption has been one of the main avenues for the development of acoustic metamaterials and metasurfaces [10, 17, 18]. Several strategies have been employed to address this challenge, both in transmission [11, 18–21] and reflection [22–24] problems: soft boundaries [16], decorated membrane panels [25–27], bubble meta-screens [28, 29], Helmholtz [19, 22, 26, 30, 31] and coiled-up [15, 17, 32–34] resonators arrangements, among others. Of particular interest is the phenomenon of slow sound [23, 35, 36], resulting from the strong dispersion around the resonances of the system. It allows both the sound speed and the inherent losses to be adjusted simply by changing the geometry and properties of the resonators.

Diffusion control using metasurfaces [37] has also attracted much interest and, in particular, Jimenez *et al.* have designed a metadiffuser based on Helmholtz resonators (HRs) capable of controlling the phase of the reflection coefficient of a surface and thus modifying the diffusion pattern [38]. An experimental proof of this design was recently performed by Ballestero *et al.* [12, 39].

Despite all this research based on slow sound, realistic applications, especially in the time domain, have not been thoroughly studied.

In this work, we propose to study analytically and numerically, to design and fabricate, and then to experimentally validate a delay line device allowing to time-delay a pulse. We first outline the paradigm underlying this work and study the influence of the geometry on the effective and scattering properties of the system. We then discuss the challenge of temporal propagation in such

metamaterials and explain the design strategy employed. Finally, we show numerical simulation and experimental results of our delay line for three different configurations.

The idea behind this work is to propose a device to be placed on the walls of a room as sketched in Fig. 1, allowing to give a sound sensation of a room larger than it really is, which is also referred to as an acoustic mirage by Norris [40]. In other words, we seek to control the phase ϕ_R of the reflection coefficient R, and thus to be able to tune the apparent group delay τ_g

$$\tau_g(\omega) = -\frac{\mathrm{d}}{\mathrm{d}\omega}\phi_R(\omega), \tag{1}$$

with ω being the angular frequency.

Since a pulse is by definition finite in time, its frequency content spreads to some extent. Thus, in order for the metasurface to delay the pulse without distorting it significantly, it must have a near-constant group delay, i.e., a near-linear phase, over the bandwidth of the pulse.

For this purpose, we consider a metasurface composed of Helmholtz resonators mounted in parallel to a slit opened to the room and backed by a rigid wall. For sake of simplicity, we show here a 1D situation consisting of 2 different HRs of dimensions given in Fig. 1(b) and Tab. I, placed in a square cross-sectional impedance tube of width $w_{ex} = 149$ mm. The walls of the impedance tube being rigid, i.e., Neumann condition applies, the considered configuration is equivalent to an infinite symmetric repetition of the unit cell as depicted in Fig. 1(b).

The strong dispersion generated in the slit above the resonators allows careful monitoring of the real and imaginary parts of the wavenumber $k(\omega)$, and thus of the group velocity $c_g = \mathrm{d}\omega/\mathrm{dRe}\{k(\omega)\}$ and dissipation ($\propto \mathrm{Im}\{k(\omega)\}$).

The dispersion by a 1 HR unit cell is calculated in steady state by the transfer matrix method (TMM) [41] and depicted in Fig. 2 (a-b) by the dotted lines. This dispersion relation does not account for the finite size of the system under study since it is derived directly from the transfer matrix elements of a single unit cell. The finite size effects of the system can be seen by additionally calculating the reflection and transmission coefficient of the entire device and then deriving the effective properties (see [41] for more details). The effective wave number and group velocity derived from the scattering parameters are thus shown in Fig. 2 (a-c). It is worth noting here, that the rigid backing, i.e., $\partial p/\partial x = 0$, imposes a mirror symmetry. The effective medium corresponding to a rigidly backed system of N resonators is equivalent to an effective medium of $2N$ resonators in transmission.

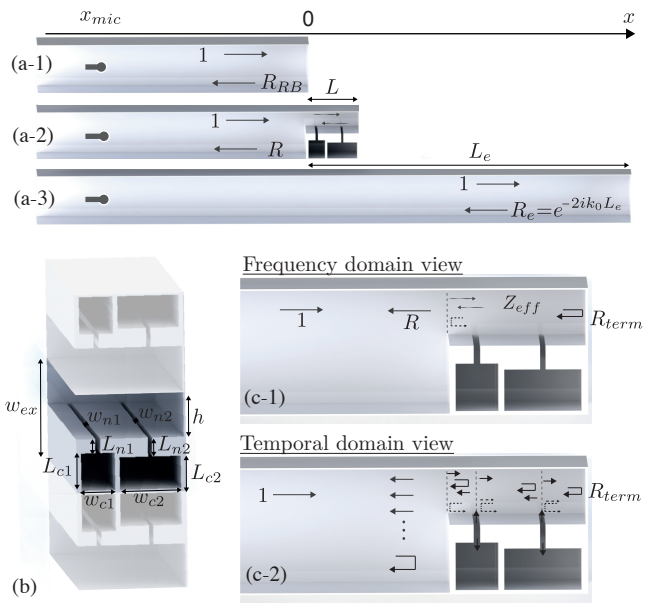

FIG. 1. (a) Schematics of the different configurations measured in a square cross-section impedance tube of width w_{ex}, in which a plane wave is impinging from the left and is reflected on a rigid wall: (a-1) configuration without the metadevice, i.e., empty tube, (a-2) configuration with the metamaterial of length L placed at the end of the rigidly backed tube, and (a-3) target configuration to be reproduced with the metamaterial. (b) Geometrical dimension of the Helmholtz resonators. (c) Differences between the permanent/frequency regime view and the temporal propagation view.

The slow sound phenomenon, which is driven by the resonator geometry, is clearly visible in Fig. 2 (c), with a subsonic group velocity in the static limit ($\omega \to 0$) and decreasing until the stop band above the HR resonance (colored in gray). In parallel, the dissipation increases near the stop band of the system, as shown by the large imaginary part of the wavenumber in Fig. 2 (b). For a given geometry, i.e., resonance frequency, we are therefore able to work with a given group velocity and amount of loss, just by selecting the frequency.

The phase of the metasurface reflection coefficient is plotted with the group delay in Fig. 2 (d-e) for $N = 1$ or 2 identical resonators (dashed and dotted-dashed black lines). Each resonator gives rise to a -2π phase jump and a group delay peak at frequencies corresponding to the Fabry-Perot resonances of the finite-depth structure. The case of two detuned resonators is also represented by the red solid lines. Although the periodicity is broken, we still have the same behavior with two group delay peaks at frequencies related to the resonance frequency of each resonator. The choice of different resonators thus facilitates the design of a metasurface with a quasi-flat group

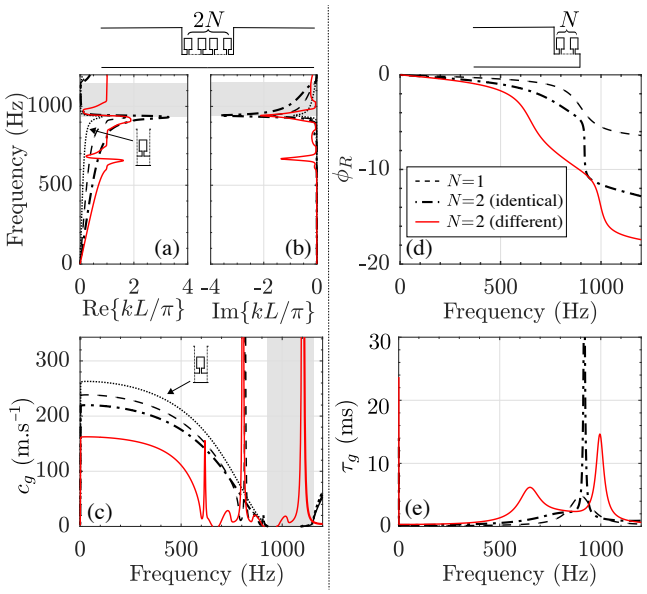

FIG. 2. [Color online] Analytically calculated effective properties of the metasurface. (a) Real and (b) imaginary parts of the normalized dispersion relation, and (c) effective group velocity. The dotted lines represent the one unit-cell effective parameters (infinite device) while the dashed, dotted-dashed and red solid curves represent the effective parameters accounting for the finite size of the device, respectively for $N = 1$, $N = 2$ with two identical unit cells, and $N = 2$ with two different HRs. (d) Phase of the reflection coefficient and (e) group delay in the rigidly backed configuration.

delay. The two group delay maxima are located in the vicinity of the open stop bands above the resonance frequency of each different HR. Note here that the sharp peaks in Fig. 2 (c) result from the inverse of the partial derivative of the non-zero flat wavenumber ($c_g = \mathrm{d}\omega/\mathrm{dRe}\{k\}$), due to the folding of the dispersion relation, in the frequency ranges between the stop bands. These regions are therefore also highly dissipative (see Fig. 2 (b)). A compromise must be found to reproduce both the right amount of loss and the time delay of a propagation over the target length.

Although effective properties and total reflectance are a good way to model and design structures in the steady state (as generally done for metamaterials and metasurfaces), they are not suitable for the time domain, as they do not account for the first reflection interferences of the transient regime required to reach the steady state. Under the steady-state condition (frequency-domain view), the design strategy would consist to impose both an impedance matching condition and a target group delay over a given frequency range by controlling the effective impedance and total reflection. Impedance matching ensures that all of the incident wave will be transmitted

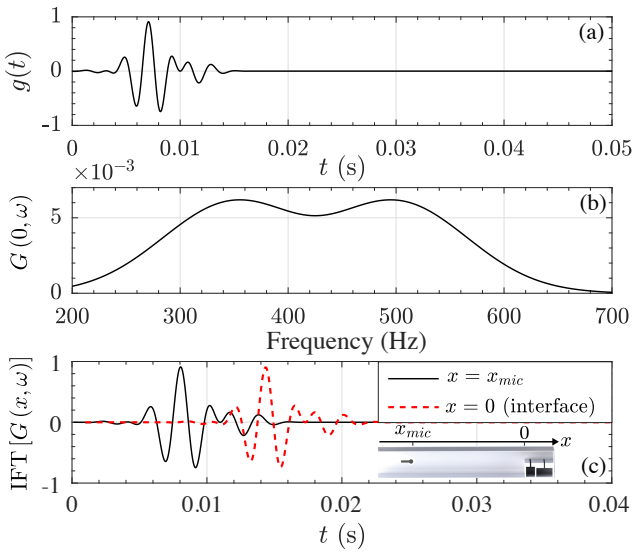

FIG. 3. [Color online] Pulse under consideration: (a) temporal signal of the pulse, (b) spectral content, and (c) propagated pulse at $x = x_{mic} = -2.6$ m, black solid line, and at the interface $x = 0$, red dashed line.

into the slit, propagate with a low group velocity, be reflected back by the rigid wall, and propagate back. The wave is therefore efficiently time-delayed due to the slow sound, as illustrated in Fig. 1 (c-1). In contrast, treating the time domain requires considering the reflection at each interface that are hidden in frequency calculations since only the total reflection is considered. In particular, the mere presence of a cross-section change at $x = 0$ generates a first direct reflection which cannot be delayed in time, as the reflected energy does not enter the metasurface.

Therefore, the design strategy adopted here is to optimize the geometry directly in the time domain for a given time propagating pulse and to use destructive interferences to minimize unwanted reflections (direct reflection at $x = 0$ and coda) and to maximize desired reflections in order to preserve the shape of the delayed pulse.

The considered pulse, see Fig. 3 (a), consists of a combination of two cosine-modulated Gaussian pulses with carrier frequencies 350 Hz and 500 Hz. The metasurface must therefore be efficient on the challenging low frequency range shown in Fig. 3 (b). We can then calculate the propagated pulse via an Inverse Fourier Transform (IFT) of the initial pulse multiplied by the total reflection coefficient sought R. As an example, we show on Fig. 3 (c) the pulse at the microphone position (black line) and at the interface ($x = 0$) after a propagation on a length of $x_{mic} = 2.6$ m (red dotted line).

To mimic the propagation of the $g(t)$ pulse over a length L_e with our device, we optimize

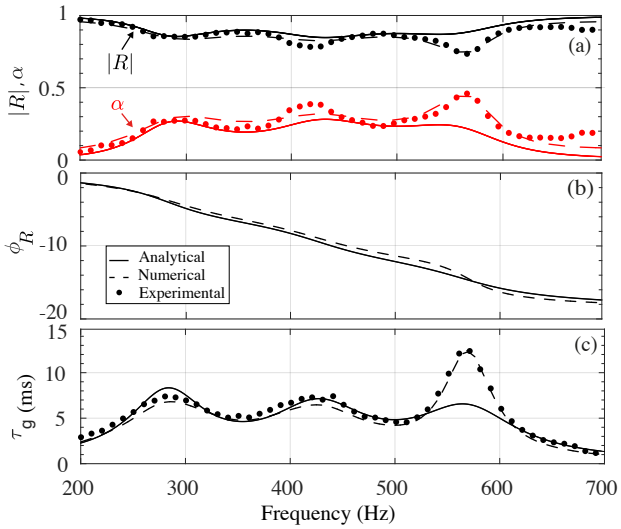

FIG. 4. [Color online] Steady state scattering properties of the metasurface optimized to reproduce a $L_e = 1$ m. (a) Reflection magnitude (black) and absorption coefficient (red), (b) phase of the reflection coefficient, and (c) apparent group delay. Solid lines represent the analytical results (TMM), dashed lines the numerical results, and dots the experimental results.

the geometry of its resonators by minimizing the difference between the target delayed pulse IFT $\left[G(\omega)\, e^{-2ik_0 L_e}\right]$ and the propagated pulse in the metasurface, modeled by its total reflection coefficient calculated by TMM, i.e., IFT $[G(\omega)\, R_{\mathrm{TMM}}]$, where $G(\omega) = \mathrm{FT}\,(g(t))$.

Figure 4 illustrates the steady-state scattering properties of the optimized metasurface reproducing a distance of 1 m and the corresponding group delay. The dimensions of the 16 cm thick metasurface of the optimized geometry are given in Tab. I. A twofold procedure is used to validate the TMM modeling. On the one hand, we numerically model the metasurface with a 3D finite element model using the viscothermal module of COMSOL Multiphysics software. A fine mesh is required for the boundary layers of all the rigid walls (cavity, neck, slit) to account for the viscothermal losses in the device with good accuracy. On the other hand, an experimental validation is performed. The metasurface is machined with 3 mm thick aluminum plates and is placed in a $w_{ex} = 149$ mm square impedance tube with a rigid backing. The scattering properties are recovered from the measurement of the microphone-to-speaker frequency responses at 4-microphone positions. The agreement between the analytical (solid), numerical (dashed line), and experimental (dots) results is very good, thus validating our analytical modeling used for the optimization process. The slight discrepancies visible around 580 Hz can be attributed to the length correction modeling for the Helmholtz resonators (see [41]).

Figure 5(a-3) shows the numerically simulated and experimentally measured outgoing temporal wave from the device. As expected and predicted by the analytical results given in Fig. 5 (a-2), the pulse is effectively delayed by 5.8 ms. This delay, highlighted by the gray horizontal arrow, corresponds to the time difference between the pulse after propagation in the metasurface and after reflection at the interface (metasurface replaced by a rigid backing at $x = 0$) shown respectively in Figs. 5 (a-3,4). Slight discrepancies are visible at the starting and end of the pulse (both in the experiments and in the simulations) and are due to several unavoidable limitations. First, although the optimization is performed over a frequency region where the dispersion is small, the Helmholtz resonator metasurfaces remain dispersive, as shown by the non-perfectly constant group delay in Fig. 5 (a-1). Second, destructive interference with early and late reflections cannot perfectly result in total wave cancellation. In addition, due to the viscothermal losses inherent to Helmholtz resonators, the amplitude of the pulse is slightly reduced. Finally, the second pulse visible in Fig. 5 (a-4) is due to the reflection on the rigid wall around the loudspeaker. Nevertheless, most of the energy remains concentrated on the targeted pulse and therefore has the potential to give the overall good feeling of a delayed pulse.

From the optimized geometry of the 1 m configuration, we then optimize the geometry to reproduce two other propagation distances $L_e = 0.75$ m and $L_e = 0.6$ m, by changing only the cavity widths w_c by a factor 0.611 and 0.42 respectively. The device thicknesses for these two configurations are therefore $L = 9.8$ cm and $L = 6.6$ cm respectively. The dimensions of the three configurations are given in Tab. I and the results are given in Figs. 5 (b-c). In each case, the optimal geometry delays the pulse by the correct time delay, $\tau_g = 4.4$ ms and 3.5 ms respectively. We can see that the steady state group delay of the optimized geometry corresponds to these values at frequencies 350 and 500 Hz, i.e., the two carrier frequencies of the pulse. Although the pulse is distorted more significantly when we linearly reduce the geometry from the first configuration, the shape and location of the pulse matches the target values. Note again here that the second pulse visible in the last row of subplots is solely due to the experimental setup. The left side of the impedance tube, on which the source is mounted, is not anechoic, which leads to a back reflection of the reflected pulse.

In conclusion, we have analytically designed in this work a metasurface capable of temporally delaying a pulse. This sub-wavelength device is able to mimic a propagation over a distance much larger than its thickness L, i.e., $L_e \approx 6.25L$ for the first configuration, $L_e \approx 7.8L$ for the second, and $L_e \approx 9L$ for the third configuration and could be reconfigurable, since a linear modification

Configurations	w_{ex}	h	w_{c1}	L_{c1}	w_{n1}	L_{n1}	a_1	w_{c2}	L_{c2}	w_{n2}	L_{n2}	a_2
HRs, dispersion relation	149 mm	68.8 mm	21.4 mm	29.1 mm	13.1 mm	45.2 mm	25.5 mm	46.7 mm	11.9 mm	2.5 mm	61.2 mm	60.7 mm
Config.1 - $L_e = 1$ m	149 mm	65.8 mm	51.3 mm	56.7 mm	7.8 mm	57 mm	92.7 mm	49.5 mm	28.7 mm	6.6 mm	28.7 mm	102.9 mm
Config. 2 - $L_e = 0.75$ m	149 mm	65.8 mm	31.3 mm	56.7 mm	7.8 mm	37 mm	56.6 mm	49.5 mm	28.7 mm	6.6 mm	28.7 mm	66.8 mm
Config. 3 - $L_e = 0.6$ m	149 mm	65.8 mm	21.6 mm	56.7 mm	7.8 mm	27.3 mm	38.9 mm	49.5 mm	28.7 mm	6.6 mm	28.7 mm	49.1 mm

TABLE I. Dimensions of the metasurface for the different configurations considered.

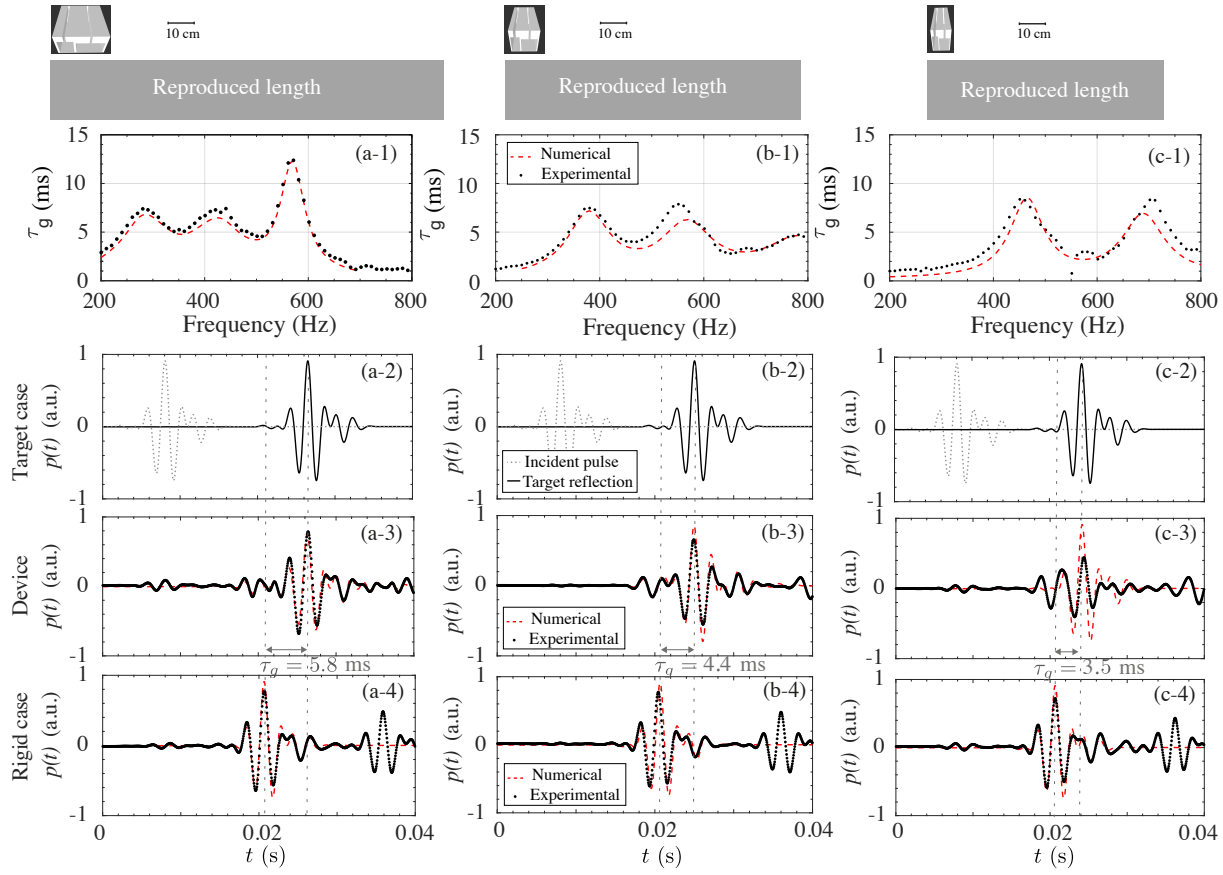

FIG. 5. [Color online] Metasurface delayed pulse for the 3 configurations considered: $L_e = 1$ m (a), 0.75 m (b), and 0.6 m (c).

(-1) steady state group delay, (-2) incident and target pulse (analytical), (-3) measured and simulated pulse delayed by the metasurface, and (-4) measured and simulated pulse reflected off a rigid wall (without metasurface). The red dashed lines and black dots represent the full-wave simulation and experimental results, respectively. The solid black lines represent the analytical target, and the thin black dotted lines the incident pulse.

of an initial geometry can reproduce several distances. As room acoustics application requires to account for the multiple reflections at each interface, the geometry optimization is performed by minimizing in the time domain the difference between the targeted pulse (propagation over a distance L_e) and the pulse after propagation in the metasurface of reflection coefficient R, determined from the TMM. We validated our analytical predictions both numerically and experimentally. We found that all three configurations reproduce well the correct group delay at the two carrier frequencies of the considered pulse and thus that the center of the pulse corresponds well to that of the target. Small discrepancies at the beginning and end of the delayed pulses, due to unavoidable dispersion and unwanted reflection, are found. However, since most of the energy of the pulse is concentrated in its center, which matches well with that of the target, the device could provide the sound feeling of the delayed pulse. In terms of prospects, a reconfigurable accordion device could be fabricated and the bandwidth of the working frequency could be extended, for example, by adding multiple slits in parallel.

This work was funded by the Metaroom Project No. ANR-18-CE08-0021 and co-funded by ANR and RCG.

---

* matthieu.mallejac@univ-lemans.fr

[1] M. Schroeder, **57**, 149 (1975).

[2] J. Jagla, P. Chervin, and J. Martin (2017) p. 3852.

[3] X. Guo, H. Lissek, and R. Fleury, Phys. Rev. Applied **13**, 014018 (2020).

[4] C. Cho, X. Wen, N. Park, and J. Li, Nature Communications **11** (2020), 10.1038/s41467-019-14124-y.

[5] T. S. Becker, D.-J. van Manen, C. M. Donahue, C. Bärlocher, N. Börsing, F. Broggini, T. Haag, J. O. Robertsson, D. R. Schmidt, S. A. Greenhalgh, and T. E. Blum, Physical Review X **8** (2018), 10.1103/physrevx.8.031011.

[6] X. Li, J. Robertsson, A. Curtis, and D.-J. van Manen, The Journal of the Acoustical Society of America **146**, 3141 (2019).

[7] T. S. Becker, N. Börsing, T. Haag, C. Bärlocher, C. M. Donahue, A. Curtis, J. O. A. Robertsson, and D.-J. van Manen, Physical Review Applied **13** (2020), 10.1103/physrevapplied.13.064061.

[8] T. Cavalieri, J. Boulvert, G. Gabard, V. Romero-García, M. Escouflaire, J. Regnard, and J.-P. Groby, Materials **13**, 4605 (2020).

[9] B. Assouar, B. Liang, Y. Wu, Y. Li, J.-C. Cheng, and Y. Jing, Nature Reviews Materials **3**, 460–472 (2018).

[10] M. Yang and P. Sheng, Annu. Rev. Mater. Res. **47**, 83 (2017).

[11] N. Jiménez, V. Romero-García, V. Pagneux, and J.-P. Groby, Sci Rep **7**, 13595 (2017).

[12] E. Ballestero, N. Jiménez, J.-P. Groby, S. Dance, H. Aygun, and V. Romero-García, Appl. Phys. Lett. **115**, 081901 (2019).

[13] S. Qu and P. Sheng, Phys. Rev. Applied **14**, 034060 (2020).

[14] Y. Zhu, A. Merkel, K. Donda, S. Fan, L. Cao, and B. Assouar, Phys. Rev. B **103**, 064102 (2021).

[15] M. Yang, S. Chen, C. Fu, and P. Sheng, Mater. Horiz. **4**, 673 (2017).

[16] H. Y. Mak, X. Zhang, Z. Dong, S. Miura, T. Iwata, and P. Sheng, Physical Review Applied **16** (2021), 10.1103/physrevapplied.16.044062.

[17] X. Cai, Q. Guo, G. Hu, and J. Yang, Appl. Phys. Lett. **105**, 121901 (2014).

[18] M. Yang, C. Meng, C. Fu, Y. Li, Z. Yang, and P. Sheng, Appl. Phys. Lett. **107**, 104104 (2015).

[19] N. Jiménez, V. Romero-García, V. Pagneux, and J.-P. Groby, Phys. Rev. B **95**, 014205 (2017).

[20] T. Lee, T. Nomura, E. M. Dede, and H. Iizuka, Phys. Rev. Applied **11**, 024022 (2019).

[21] V. Romero-García, N. Jiménez, J.-P. Groby, A. Merkel, V. Tournat, G. Theocharis, O. Richoux, and V. Pagneux, Phys. Rev. Applied **14**, 054055 (2020), arXiv: 2007.08393.

[22] V. Romero-García, G. Theocharis, O. Richoux, A. Merkel, V. Tournat, and V. Pagneux, Sci Rep **6**, 19519 (2016).

[23] N. Jiménez, W. Huang, V. Romero-García, V. Pagneux, and J.-P. Groby, Appl. Phys. Lett. **109**, 121902 (2016).

[24] Y. Aurégan, Appl. Phys. Lett. **113**, 201904 (2018).

[25] J. Mei, G. Ma, M. Yang, Z. Yang, W. Wen, and P. Sheng, Nat Commun **3**, 756 (2012).

[26] P. Wei, C. Croënne, S. Tak Chu, and J. Li, Appl. Phys. Lett. **104**, 121902 (2014).

[27] M. Yang, Y. Li, C. Meng, C. Fu, J. Mei, Z. Yang, and P. Sheng, Comptes Rendus Mécanique **343**, 635 (2015).

[28] V. Leroy, A. Strybulevych, M. Lanoy, F. Lemoult, A. Tourin, and J. H. Page, Phys. Rev. B **91**, 020301 (2015).

[29] M. Lanoy, R.-M. Guillermic, A. Strybulevych, and J. H. Page, Appl. Phys. Lett. **113**, 171907 (2018).

[30] V. Romero-García, G. Theocharis, O. Richoux, and V. Pagneux, The Journal of the Acoustical Society of America **139**, 3395 (2016).

[31] V. Romero-García, N. Jiménez, G. Theocharis, V. Achilleos, A. Merkel, O. Richoux, V. Tournat, J.-P. Groby, and V. Pagneux, Comptes Rendus. Physique **21**, 713 (2021).

[32] Y. Li and B. M. Assouar, Appl. Phys. Lett. **108**, 063502 (2016).

[33] C. Zhang and X. Hu, Phys. Rev. Applied **6**, 064025 (2016).

[34] K. Donda, Y. Zhu, S.-W. Fan, L. Cao, Y. Li, and B. Assouar, Applied Physics Letters **115**, 173506 (2019), https://doi.org/10.1063/1.5122704.

[35] J.-P. Groby, R. Pommier, and Y. Aurégan, The Journal of the Acoustical Society of America **139**, 1660 (2016).

[36] J.-P. Groby, W. Huang, A. Lardeau, and Y. Aurégan, Journal of Applied Physics **117**, 124903 (2015).

[37] Y. Zhu, X. Fan, B. Liang, J. Cheng, and Y. Jing, Phys. Rev. X **7**, 021034 (2017).

[38] N. Jiménez, T. J. Cox, V. Romero-García, and J.-P. Groby, Sci Rep **7**, 5389 (2017).

[39] E. Ballestero, N. Jiménez, J.-P. Groby, H. Aygun, S. Dance, and V. Romero-García, Appl. Phys. Lett. **119**, 044101 (2021).

[40] A. N. Norris, The Journal of the Acoustical Society of America **125**, 839 (2009).

[41] S. M., The supplemental presents the analytical modeling of the metasurface, recalls how to derive the dispersion relation from a single unit cell, as well as the effective wave number to, and presents the experimental results obtained from the optimized geometry of two other configurations reproducing a distance of 0.75 m and 0.6 m..